Hindawi
Journal of Nanomaterials
Volume 2017, Article ID 7251725, 7 pages
https://doi.org/10.1155/2017/7251725

Research Article

Nanoferrofluid Materials: Advanced Structure Monitoring Using Optical Transmission in a Magnetic Field

Serhii Shulyma, Bogdan Tanygin, Valery Kovalenko, and Michail Petrychuk

Department of Radiophysics, Taras Shevchenko Kyiv National University, 4G, Acad. Glushkov Ave., Kyiv 03187, Ukraine

Correspondence should be addressed to Serhii Shulyma; kiw_88@mail.ru

Received 24 December 2016; Revised 20 March 2017; Accepted 12 April 2017; Published 10 May 2017

Academic Editor: Balachandran Jeyadevan

The optical transmission of a thin ferrofluid layer was investigated at various optical radiation wavelengths. The turning on of the durable external magnetic field pulse leads to nonmonotonic changes of the optical transmission value with minimal value during the field pulse. This phenomenon is related to the formation of columnar nanoparticle aggregates and transformation in the ferrofluid bulk. It was shown that time interval corresponding to the optical transmission minimum is proportional to the laser wavelength, which can be explained with Mie-like optical extinction on the ferrofluid aggregates and its dependence on the diameters of columnar aggregates. Hence, a simple experimental approach was proposed to measure and control the ferrofluid aggregates diameters in submicron spatial dimension ranges. Particularly, this approach could be used for the formation of composite nanomaterials consisting of polymers and magnetic nanoparticles with controlled structural parameters. These materials could be reused after parameters changes (e.g., lattice constant, aggregate size, and magnetic permeability tensor) with a heating/cooling cycle without the need for preparation of a new material from scratch.

1. Background

There are a large number of recent scientific reports dedicated to new nanomaterials, their synthesis methods, structures, and applications in various sectors, such as electronics [1, 2], energetics [3, 4], and life sciences [5, 6]. Manufacturing of magnetic single-domain nanoparticles has been an advanced subject of research in the modern nanophysics that are typically suspended in a carrier fluid, forming a ferrofluid (FF). Ferrofluids combine both liquid and magnetic characters [7].

The new century FF topicality revival is related to new application trends: magnetic targeted in vivo drug delivery [8, 9], local tumor hyperthermia [10], solid body surface polishing [11], programmable lithography mask [12], and others [13, 14]. The FF properties (magnetic permeability tensor, saturation magnetization, viscosity, and other properties) could be varied by its integral parts changes, for instance, in the carrier liquid and the type and concentration of nanoparticles. However, even without modification of such components, the FF properties could vary via magnetic nanoparticle aggregation phenomenon. There are two major kinds of FFs [15]: highly stabilized colloid of magnetic single-domain nanoparticles ("classical" FF) [16] and nonclassical FF [17]. Without an external magnetic field, the classical FF may contain only submicron primary aggregates with confined magnetic flux [18]. Oppositely, nonclassical FF contains large aggregates visible in an optical microscope [18, 19]. Application of an external magnetic field reversibly produces visible aggregates in both types of a FF [16, 17, 19–21]. Electrical field [22] and optical radiation [23] may also lead to formation of reversible aggregates. Magnetic field could produce 1D and 2D long-range ordered self-organized FF aggregate structures, including visible ones [14, 16, 24, 25]. They can be used for the formation of micro- and nanostructured magnetic materials, including liquid photonic crystals [25]. The reversible formation of a periodical magnetic aggregate structure could be used for composite materials with specifically assigned properties and ability to change properties later for specific applications. Particularly, the magnetic field sweep rate variation could be used to change the columnar aggregate diameter [26].

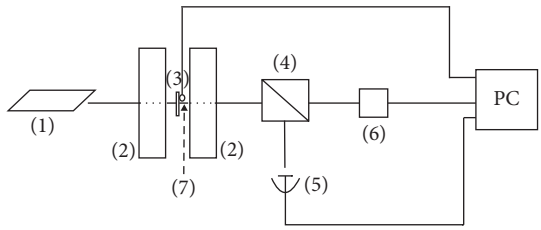

Figure 1: Optical transmission experimental setup: He-Ne laser (#1), electromagnet (#2), FF sample (#3), beam splitter (#4), photodetector (#5), CMOS USB camera (#6), digital thermometer (#7), and personal computer (PC).

Investigations on the internal FF structure and its transformation are performed through various techniques of optical methods [16, 23, 27], small-angle neutron scattering [28, 29], ultrasound dissipation [30], and diffusion coefficient determination [31]. In the present work, we implemented experimental method of optical extinction measurements in an external magnetic field [16].

It has been shown that timestamp of a minimal optical extinction corresponds to columnar aggregates diameter in the order of magnitude of a laser wavelength [16]. The main aim of the present work was to study the corresponding spectral dependence. The observations may reveal a quantitative information about the FF submicron structure that can be used, particularly, for preparation of composite materials.

2. Methods

Initial FF sample contained Fe_3O_4 nanoparticle suspended in a kerosene prepared using Elmore method [32]. Oleic acid coating was performed to stabilize the nanoparticles. The mean diameter of the magnetite nanoparticles was determined using electronic microscopic as $\langle d \rangle \approx 11.5$ nm with corresponding average hydrodynamic diameter calculated as $\langle d_H \rangle \approx 15.5$ nm [16]. The magnetite volume fraction of the FF sample was observed as $\varphi_V = 1.2\%$, which corresponds to an increase in FF sedimentation stability. Experimental procedure consisted of FF samples entrapped into round-shaped glass container with a diameter of 13 mm, which formed between a microscope slide and a cover slip as a gap. Such a shape was selected for decrease of the magnetic field spatial inhomogeneity, which numerically was estimated to be smaller than 1%. After entering FF into container, it was hermetically sealed by liquid polymer. The container thickness h was controlled and restricted using copper wires with known diameters. In this work we used 50 μm FF container. The optical transmission experimental setup is presented on Figure 1.

Different sources of optical radiation (#1) with a beam diameter of ~1 mm were used: He-Ne red laser with parameters of $\lambda_R = 630$ nm (1.5 mW) and solid state lasers of green $\lambda_G = 530 \pm 10$ nm (18 mW), infrared $\lambda_{IR} = 1060 \pm 10$ nm (12 mW), and blue $\lambda_B = 450 \pm 10$ nm (140 mW). The electromagnet (#2) was inducing a magnetic field along the optical radiation direction of Z. The FF sample (#3) was placed in the gap between electromagnet poles and the microscope slide (plane XY) oriented orthogonally to magnetic field force lines and incident laser beam. The direction of optical radiation propagation was aligned normal (axis Z) to the FF sample plane XY and coincided with the external magnetic field produced by an electromagnet, which allowed changing the applied magnetic field magnitude in the range of 0–3 kOe. The magnetic field pulse was produced using an electromechanical switch. The laser beam was directed to the beam splitter (#4), allowing the simultaneous transmission coefficient measurement and the FF layer visual observation with a photodetector (#5) and CMOS USB camera (#6), respectively. Research on the FF layer optical transmission changes was performed using sole durable magnetic field pulses ($\tau_{pulse} \sim 200$ s). The photodetector electric signal was transmitted to a personal computer (PC) using a voltage registration with an external analog-to-digital converter Triton 3000 U with time samples divisions of 150 ms. Temperature changes in FF samples during experiments were controlled by digital thermometer DS1820 (#7). The laser switched off after each measurement until temperature became equal to room temperature. The FF sample probing ray optical extinction measurement technique was used at various wavelengths [16]. Recovery of the initial state FF submicron structure was achieved in a long enough time interval between sequential measurements (~5 min).

3. Results and Discussion

The variations of optical transmission extinction value in a magnetic field have been described using the relative optical transmission coefficient $T = I_1/I_2$, where I_2 (I_1) is an optical radiation intensity that passed the FF sample before (after) turning on the magnetic field pulse. It was shown [33, 34] that long-term magnetic field pulse application to either thin ionic or surfactant-stabilized FF layers [16, 35] leads to an emergence of an optical extinction trend inversion (OETI) phenomenon, which could be described in detail as follows. The FF transparency decreases after the magnetic field pulse rising edge (timestamp τ_0) for the time interval τ_1. Then, the FF transparency starts growing until the magnetic field falling edge τ_0' (Figure 2). The magnetic field switch-off was followed by a recovery of the initial optical transmission and returns internal structure to the original state.

The OETI phenomenon has been investigated at four different wavelengths (λ_B, λ_G, λ_R, and λ_{IR}) and different magnetic field magnitudes. Identical latter values correspond to different experimentally observed OETI timestamps of τ_1^B, τ_1^G, τ_1^R, and τ_1^{IR} (Figure 2). Corresponding dependencies on the magnetic field magnitude are provided in Figure 3.

Due to the fact that lasers with different powers were used in our investigation, we monitored temperature in the FF samples during our measurements. Corresponding dependencies are provided in Figure 4.

The OETI phenomenon has been investigated for different magnetite volume fraction (Figure 5). As one can be seen from Figure 5, this phenomenon exists only at some φ_V values. The OETI phenomenon was not observed for much diluted FF samples ($\varphi_V \leq 0.3\%$) and for samples with

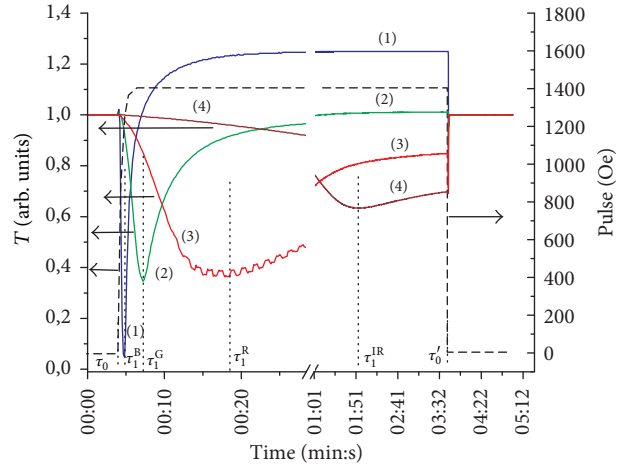

FIGURE 2: Temporal dependencies of optical transmission T changes under magnetic field applied: $H = 1400$ Oe at laser wavelengths of λ_B (1), λ_G (2), λ_R (3), and λ_{IR} (4). The value T approximately equals 1 for all dependencies after magnetic field pulse falling edge. First local T minimum corresponds to the OETI point τ_1.

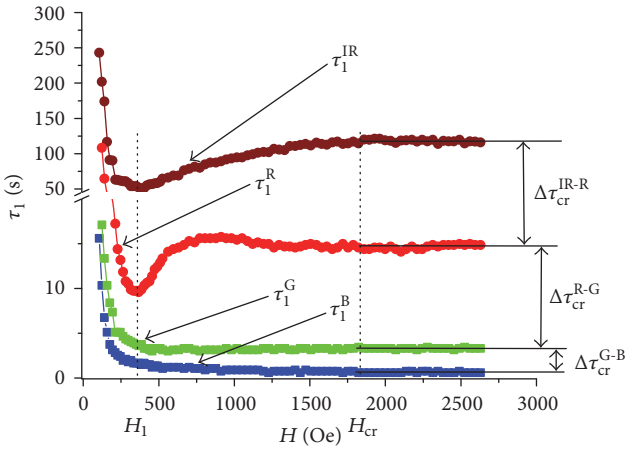

FIGURE 3: Optical extinction trend inversion dependencies of τ_1^B, τ_1^G, τ_1^R, and τ_1^{IR} on the magnetic field pulse magnitude at laser wavelengths of λ_B, λ_G, λ_R, and λ_{IR}, respectively.

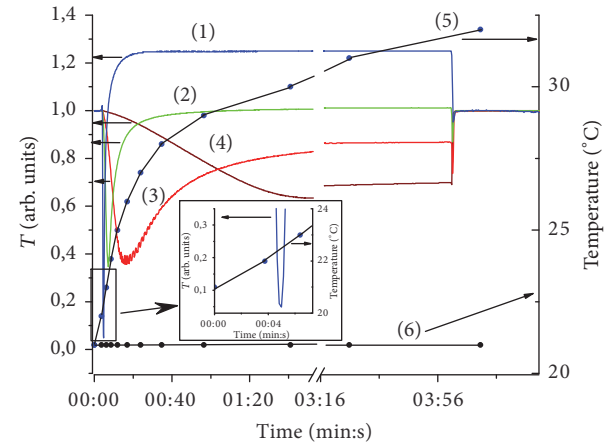

FIGURE 4: Temporal dependencies of the temperature (right axis) in the FF samples during optical transmission T measurements (left axis: at the laser wavelengths of λ_B (1), λ_G (2), λ_R (3), and λ_{IR} (4)) under the magnetic field applied ($H = 1400$ Oe): the temperature is changing under the laser irradiation influence with λ_B (5) and with λ_G, λ_R, and λ_{IR} (6). The inset shows more detailed temporal dependencies of the temperature in the specimen during optical transmission measurements for laser with λ_B during first 7 seconds.

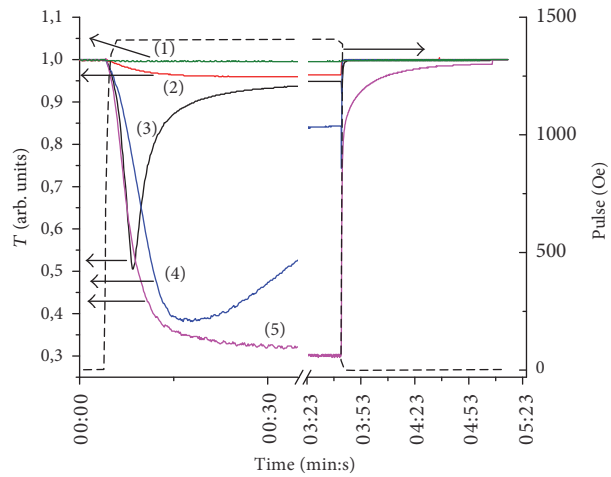

FIGURE 5: Temporal dependencies of optical transmission T changes for λ_R under magnetic field applied ($H = 1400$ Oe) for different magnetite volume fraction (φ_V): $\varphi_V = 0.2\%$ (1), $\varphi_V = 0.3\%$ (2), $\varphi_V = 0.6\%$ (3), $\varphi_V = 1.2\%$ (4), and $\varphi_V = 2\%$ (5).

magnetite volume fraction more than 2% (Figure 5). Such behavior requires more detailed study, which will be provided in our further works.

As it was shown [16, 17, 36], mostly larger (5%⋯10% mole fraction) magnetic nanoparticles produce aggregates. All other polydisperse FF nanoparticles usually perform within individual Brownian motion. In the case of classical magnetite FF, the large nanoparticle hydrodynamic diameter is given as $\langle d_H^L \rangle \approx 25.6$ nm [16]. Without the external magnetic field, these nanoparticles form sole primary aggregates without long-range ordering distributed over FF sample bulk [18, 37]. Turning on the magnetic field destroys the primary aggregates and forms 1D chain aggregates aligned with the field direction (axis Z). According to Langevin dynamics simulation [16], initially short chains are formed after ~1 ms, then passing additional ~10 ms, they fuse and form long chains (Figure 6(a)) with a length of L restricted only by the FF container size. Further development of these structures exposed to the external magnetic field leads to their lateral aggregation and formation of thicker columnar aggregates [35, 38] (Figure 6(b)) with a thickness (which could be treated as a diameter L assuming $D \gg \langle d_H^L \rangle$) growing [16] (Figure 6(c)). This process is more durable and can be observed in real time. The lateral aggregation corresponds to the average large nanoparticles flow coming to the aggregate $J \equiv \langle d^2N/dSdt \rangle$, where dN is an average number of nanoparticles passing the columnar aggregate surface area dS in a time dt. Here, the flow J is averaged over

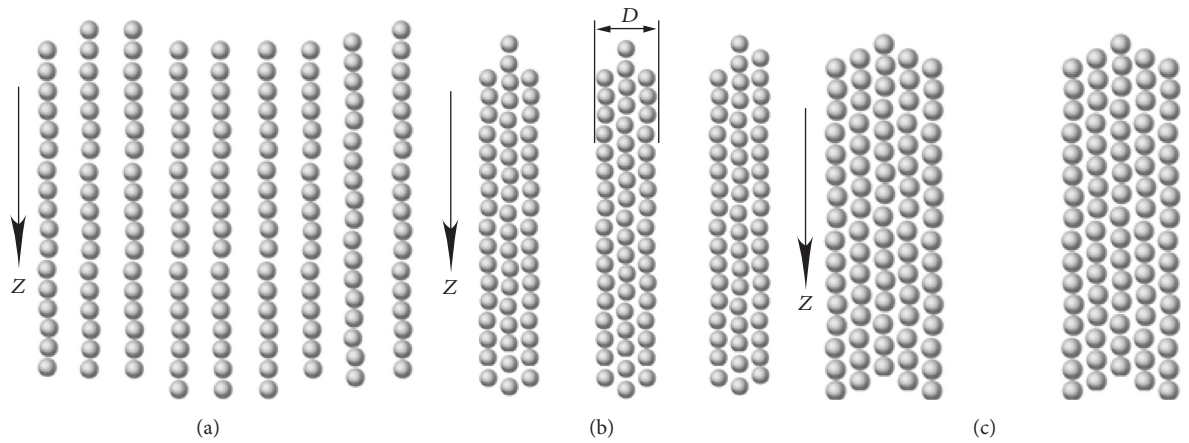

Figure 6: Schematic of the formation and growth of columnar aggregates (from *large* nanoparticles) in an external magnetic field strength ($\mathbf{H} \parallel Z$). (a) Long chains of magnetic nanoparticles in an external magnetic field. (b) Lateral aggregation of long chains and formation of thicker columnar aggregates with increasing of external magnetic field and/or over time. (c) Further lateral aggregation of columnar aggregates.

sole nanoparticles, primary aggregates attaching, and the columnar aggregates fusion. The columnar aggregate volume V_a growth depends on the nanoparticle mean volume V_0 and corresponding free space packing factor κ [39] as follows:

$$\frac{dV_a}{dt} = \frac{V_0}{\kappa} \int J \, dS, \tag{1}$$

where the integration is made over the columnar aggregate surface. Corresponding approximate diameter growth can be presented by the following equation:

$$\frac{dD}{dt} = \frac{\pi \left\langle d_H^L \right\rangle^3 J}{3\kappa}, \tag{2}$$

where $\kappa \approx 0.74$ in case of close packing of the cubic or hexagonal type [39]. Other packing types include quasicrystal-like structure, corresponding to smaller κ values. Particularly, random close packing corresponds to the value $\kappa \approx 0.634$ [40]. The timestamp τ_1 (Figure 2) complies with the condition of $D = D_0 \sim \lambda$ [16, 41]:

$$D_0 = \int_0^{\tau_1} \frac{\pi \left\langle d_H^L \right\rangle^3 J}{3\kappa} dt. \tag{3}$$

Considering the optical extinction on sole nanoparticles and primary aggregates, further increase in columnar aggregates' size means a decrease in total scattering centers cross section (perpendicular to the laser beam) area, resulting in an overall optical transmission growth (Figure 2). This phenomenon is known as the shadowing effect. The magnetic field turning off leads to aggregates destruction by the Brownian motion and a steric or entropic nanoparticles' repulsion [42]. The nanostructure returns to the original state passing the residual OETI which had been analyzed in [16].

The relative optical transmission coefficient T could take values larger than 1 before turning off the magnetic field for the λ_B and λ_G wavelength cases (Figure 2). This phenomenon can be related to the strong shortwave optical dissipation in FF [23]. It is important to note that the carrier liquid itself (kerosene in the present case) does not possess such properties. Passing of the OETI leads to a reduction of the separate nanoparticles concentration around bulk columnar aggregates and, consequently, the effect [23] reduction. An aggregation effect at the end of the magnetic field pulse increases the difference between FF and its carrier liquid.

In scope of the given time frames, turning off the magnetic field leads to FF aggregates destruction in a quite fast manner and almost simultaneously (in a time of ~1 s). This is concluded from the optical transmission coefficient value of $T \approx 1$ for all the four wavelengths (Figure 3). Hence, speeds of aggregates formation are different for λ_B, λ_G, λ_R, and λ_{IR} wavelengths. However, the speeds of their destruction are almost identical. In the absence of the time reversal symmetry transformation ($R \cdot t \to -t$), this is an indicative of strong dissipative nature of the given system. Moreover, according to graph in Figure 2, the FF aggregates with diameters in the approximate range of 400–1000 nm are formed quite slowly (~1–100 s) and destructed much faster (in a time of ~1 s).

At the same external magnetic field strength (Figure 2) for all its researched values (Figure 3), the order of $\tau_1^B < \tau_1^G < \tau_1^R < \tau_1^{IR}$ was found effective. Hence, the same initial and boundary conditions (magnetic field pulse parameters, FF dispersed phase volume concentration, carrier liquid viscosity, and investigated samples geometrical dimensions) correspond to simultaneous growth or decrease of τ_1 and λ; that is, $d\tau_1/d\lambda > 0$. This observation is a justification of the lateral fusion of chain and columnar aggregates in a magnetic field (Figure 6).

Minimal values of $\tau_1^{(R)}$ and $\tau_1^{(IR)}$ dependencies $\tau_1(H)$ correspond to almost identical values for the magnetic field strength of $H_1 \approx 400$ Oe (Figure 3). This peculiarity can be related to the FF aggregates "compression," for example, in a transition from nondense structures (at small κ value) to

Table 1: Increase in average aggregates velocities at various periods after turning on magnetic field pulse.

$i-j$	$\Delta\lambda_{i-j}$ (nm)	$\Delta\tau_{cr}^{i-j}$ (s)	$\overline{v_{cr}^{i-j}}$ (nm/s)	Δt (s)
G-B	≈80	2.7	≈30	$[0.6\cdots3.3]$
R-G	≈100	11.7	≈9	$[3.3\cdots15]$
IR-R	≈430	102	≈4	$[15\cdots117]$

either random close packing or the close packing structure at H_1 regardless of the specific value of $D \sim \lambda$ at $t = \tau_1$. The wavelengths of λ_B and λ_G optical radiations do not reveal this minimum value. Corresponding aggregates at τ_1 are smaller and increase in magnetic field driven aggregate growth velocity providing a much stronger effect compared to the compression, resulting in larger negative values of $d\tau_1/dH$ in shorter waves.

Achievement of a critical value of $H_{cr} \approx 1700$ Oe corresponds to limit τ_1 values to τ_{cr}^{B}, τ_{cr}^{G}, τ_{cr}^{R}, and τ_{cr}^{IR} (Figure 3). This can be related to a depletion of sole large magnetic Fe_3O_4 nanoparticles and primary aggregates in the environment surrounding the columnar aggregates at stronger magnetic fields. Hence, all large particles are ordered in the columnar aggregates starting from H_{cr} field strength.

The optical transmission at wavelength λ_R corresponds to small oscillations of the optical transmission value (Figure 2). This can be related to the light interference on aggregates [23, 41]. This result has been observed only for the red laser due to its better spectral properties. Oscillations $T(t)$ correspond to the columnar aggregates motion in the laser beam cross section during their fusion. Their 2D close packing hexagonal long-range order is kept unchanged but the lattice constant increases, as it was observed even with the optical microscope [16].

As an application of the given results, average aggregates growing velocity could be determined as dD/dt in the FF layer at $H \geq H_{cr}$:

$$\overline{v_{cr}^{i-j}} = \frac{\Delta\lambda_{i-j}}{\Delta\tau_{cr}^{i-j}} = \frac{\lambda_i - \lambda_j}{\tau_{cr}^{i} - \tau_{cr}^{j}}, \quad (4)$$

where λ_i and λ_j are adjacent laser wavelengths; indices i, j could take values of B, G, R, or IR; and τ_{cr}^{i} and τ_{cr}^{j} are corresponding critical limit values of τ_1 (Figure 3). The average aggregates growth velocities for different period of Δt after turning on the magnetic field pulse are shown in Table 1.

Decrease of the growing velocity value is related to large nanoparticles' depletion in a FF environment and the corresponding condition of $dJ/dt < 0$. The obtained information about the aggregates growth velocity could be used to practically control the FF submicron structure and, consequently, its static and dynamic physical properties, including optical and magnetic properties (magnetic permeability tensor, diffraction properties, photonic crystal parameters, and others). Usage of a reversible polymer material as a carrier liquid provides a restorable FF parameters' control. Particularly, a reversible polymer, which can make transition between liquid state and solid state, can be applied [43].

4. Conclusion

In summary, the optical transmission of thin FF layer at various wavelengths was investigated. Durable external magnetic field pulse produces extinction trend inversion during the pulse. Turning off the magnetic field recovers the FF structure to the original state. This behavior is related to the emergence and growth of the FF columnar aggregates consisting of magnetic nanoparticles. Temporal parameters of the optical extinction give a tool for the qualitative and quantitative determination of FF submicron long-range structure, which can be used for production of composite materials with changeable and controllable physical structures and reversible physical properties in a practical application. The OETI phenomenon exists only at some φ_V values.

Abbreviations

FF: Ferrofluid
OETI: Optical extinction trend inversion.

Conflicts of Interest

The authors declare that they have no conflicts of interest.

Authors' Contributions

Serhii Shulyma conceived the idea of the study and designed and conducted all experiments. Serhii Shulyma and Michail Petrychuk fabricated samples. Bogdan Tanygin carried out theoretical interpretation of the experimental results. Serhii Shulyma, Bogdan Tanygin, and Valery Kovalenko wrote the manuscript. All authors critically read and contributed to the manuscript preparation. All authors read and approved the final manuscript.

Acknowledgments

The authors would like to acknowledge Dr. Saeed Doroudiani for useful suggestions and editing the manuscript. They thank Dr. Vladimir Sokhatskiy, Dr. Alexander Klimov, and Dr. Yevgen Oberemok for using their laboratory equipment. They are grateful to Mrs. Daria Tanygina for assistance in processing of images.

References

[1] D. Jariwala, V. K. Sangwan, L. J. Lauhon, T. J. Marks, and M. C. Hersam, "Carbon nanomaterials for electronics, optoelectronics, photovoltaics, and sensing," *Chemical Society Reviews*, vol. 42, pp. 2824–2860, 2013.

[2] T. Chen and L. Dai, "Flexible supercapacitors based on carbon nanomaterials," *Journal of Materials Chemistry A*, vol. 2, no. 28, pp. 10756–10775, 2014.

[3] J. Peet, A. J. Heeger, and G. C. Bazan, "'Plastic' solar cells: self-assembly of bulk heterojunction nanomaterials by spontaneous phase separation," *Accounts of Chemical Research*, vol. 42, no. 11, pp. 1700–1708, 2009.

[4] D. Derkacs, W. V. Chen, P. M. Matheu, S. H. Lim, P. K. L. Yu, and E. T. Yu, "Nanoparticle-induced light scattering for improved performance of quantum-well solar cells," *Applied Physics Letters*, vol. 93, no. 9, Article ID 091107, 2008.

[5] A. Solanki, J. D. Kim, and K.-B. Lee, "Nanotechnology for regenerative medicine: nanomaterials for stem cell imaging," *Nanomedicine*, vol. 3, no. 4, pp. 567–578, 2008.

[6] D.-H. Kim, N. Lu, R. Ghaffari, and J. A. Rogers, "Inorganic semiconductor nanomaterials for flexible and stretchable bio-integrated electronics," *NPG Asia Materials*, vol. 4, no. 4, article no. e15, 2012.

[7] R. E. Rosensweig, *Ferrohydrodynamics*, Dover Publication, New York, NY, USA, 2013.

[8] Z. P. Aguilar, Y. Aguilar, H. Xu et al., "Nanomaterials in medicine," *ECS Transactions*, vol. 33, pp. 69–74, 2010.

[9] A. S. Lübbe, C. Bergemann, W. Hunt et al., "Preclinical experiences with magnetic drug targeting: tolerance and efficacy," *Cancer Res*, vol. 56, pp. 4694–4701, 1996.

[10] A. Jordan, R. Scholz, P. Wust, H. Fähling, and R. Felix, "Magnetic fluid hyperthermia (MFH): cancer treatment with AC magnetic field induced excitation of biocompatible superparamagnetic nanoparticles," *Journal of Magnetism and Magnetic Materials*, vol. 201, no. 1–3, pp. 413–419, 1999.

[11] K. Shimada, S. Shuchi, H. Kanno, Y. Wu, and S. Kamiyama, "Magnetic cluster and its applications," *Journal of Magnetism and Magnetic Materials*, vol. 289, pp. 9–12, 2005.

[12] B. B. Yellen, G. Friedman, and K. A. Barbee, "Programmable self-aligning ferrofluid masks for lithographic applications," *IEEE Transactions on Magnetics*, vol. 40, no. 4, pp. 2994–2996, 2004.

[13] J. V. I. Timonen, M. Latikka, O. Ikkala, and R. H. A. Ras, "Free-decay and resonant methods for investigating the fundamental limit of superhydrophobicity," *Nature Communications*, vol. 4, article 2398, 2013.

[14] J. V. I. Timonen, M. Latikka, L. Leibler, R. H. A. Ras, and O. Ikkala, "Switchable static and dynamic self-assembly of magnetic droplets on superhydrophobic surfaces," *Science*, vol. 341, no. 6143, pp. 253–257, 2013.

[15] M. I. Shliomis, "Magnetic fluids," *Uspekhi Fizicheskikh Nauk*, vol. 112, pp. 427–458, 1974 (Russian).

[16] S. I. Shulyma, B. M. Tanygin, V. F. Kovalenko, and M. V. Petrychuk, "Magneto-optical extinction trend inversion in ferrofluids," *Journal of Magnetism and Magnetic Materials*, vol. 416, pp. 141–149, 2016.

[17] B. M. Tanygin, S. I. Shulyma, V. F. Kovalenko, and M. V. Petrychuk, "Ferrofluid nucleus phase transitions in an external uniform magnetic field," *Chinese Physics B*, vol. 24, no. 10, Article ID 104702, 2015.

[18] B. M. Tanygin, V. F. Kovalenko, M. V. Petrychuk, and S. A. Dzyan, "Molecular dynamics study of the primary ferrofluid aggregate formation," *Journal of Magnetism and Magnetic Materials*, vol. 324, no. 23, pp. 4006–4010, 2012.

[19] V. F. Kovalenko, M. V. Petrychuk, B. M. Tanygin, and S. I. Shulyma, Ferrofluid aggregates phase transitions in the planar magnetic field. In: arXiv. 2014. https://arxiv.org/abs/1404.5541.

[20] S. Taketomi, H. Takahashi, N. Inaba, and H. Miyajima, "Experimental and theoretical investigations on agglomeration of magnetic colloidal particles in magnetic fluids," *Journal of the Physical Society of Japan*, vol. 60, no. 5, pp. 1689–1707, 1991.

[21] E. A. Peterson and D. A. Krueger, "Reversible, field induced agglomeration in magnetic colloids," *Journal of Colloid And Interface Science*, vol. 62, no. 1, pp. 24–34, 1977.

[22] K. V. Erin, "Formation and electrooptic investigation of the near-electrode space charge in colloidal solutions of magnetite in liquid dielectrics," *Technical Physics*, vol. 53, no. 4, pp. 522–525, 2008.

[23] B. Hoffmann and W. Köhler, "Reversible light-induced cluster formation of magnetic colloids," *Journal of Magnetism and Magnetic Materials*, vol. 262, no. 2, pp. 289–293, 2003.

[24] S. Y. Yang, Y. P. Chiu, B. Y. Jeang, H. E. Horng, C.-Y. Hong, and H. C. Yang, "Origin of field-dependent optical transmission of magnetic fluid films," *Applied Physics Letters*, vol. 79, no. 15, pp. 2372–2374, 2001.

[25] S. Y. Yang, H. E. Horng, Y. T. Shiao, C.-Y. Hong, and H. C. Yang, "Photonic-crystal resonant effect using self-assembly ordered structures in magnetic fluid films under external magnetic fields," *Journal of Magnetism and Magnetic Materials*, vol. 307, no. 1, pp. 43–47, 2006.

[26] C.-Y. Hong, "Field-induced structural anisotropy in magnetic fluids," *Journal of Applied Physics*, vol. 85, no. 8, pp. 5962–5964, 1999.

[27] J-C. Bacri and D. Salin, "Optical scattering on ferrofluid agglomerates," *Journal de Physique Letttres*, vol. 43, pp. 771–777, 1982.

[28] V. I. Petrenko, M. V. Avdeev, V. M. Garamus, L. A. Bulavin, V. L. Aksenov, and L. Rosta, "Micelle formation in aqueous solutions of dodecylbenzene sulfonic acid studied by small-angle neutron scattering," *Colloids and Surfaces A*, vol. 369, no. 1–3, pp. 160–164, 2010.

[29] V. I. Petrenko, V. L. Aksenov, M. V. Avdeev et al., "Analysis of the structure of aqueous ferrofluids by the small-angle neutron scattering method," *Phys Solid State*, vol. 52, pp. 974–978, 2010.

[30] V. V. Gogosov, S. I. Martynov, S. N. Tsurikov, and G. A. Shaposhnikova, "Propagation of ultrasound in a magnetic liquid II. Analysis of experiments. Determination of the sizes of aggregates," *Magnetohydrodynamic*, vol. 23, pp. 241–247, 1988.

[31] V. I. Drozdova, "Particles aggregation influence on an extinction and dichroism of ferrofluids," in *Physical properties of ferrofluid*, M. I. Shliomis, Ed., Sverdlovsk: UNC AN SSSR, pp. 34–41, 1983.

[32] W. C. Elmore, "Ferromagnetic colloid for studying magnetic structures," *Physical Review*, vol. 54, no. 4, pp. 309–310, 1938.

[33] J. Li, X. Liu, Y. Lin et al., "Field modulation of light transmission through ferrofluid film," *Applied Physics Letters*, vol. 91, no. 25, Article ID 253108, 2007.

[34] J. Li, X. Liu, Y. Lin, X. Qiu, X. Ma, and Y. Huang, "Field-induced transmission of light in ionic ferrofluids of tunable viscosity," *Journal of Physics D: Applied Physics*, vol. 37, no. 24, pp. 3357–3360, 2004.

[35] J. M. Laskar, J. Philip, and B. Raj, "Experimental evidence for reversible zippering of chains in magnetic nanofluids under external magnetic fields," *Physical Review E*, vol. 80, Article ID 041401, 2009.

[36] A. O. Ivanov, "Phase separation in bidisperse ferrocolloids," *Journal of Magnetism and Magnetic Materials*, vol. 154, no. 1, pp. 66–70, 1996.

[37] M. Yoon and D. Tománek, "Equilibrium structure of ferrofluid aggregates," *Journal of Physics Condensed Matter*, vol. 22, no. 45, Article ID 455105, 2010.

[38] C. Rablau, P. Vaishnava, C. Sudakar, R. Tackett, G. Lawes, and R. Naik, "Magnetic-field-induced optical anisotropy in ferrofluids: a time-dependent light-scattering investigation," *Physical Review E—Statistical, Nonlinear, and Soft Matter Physics*, vol. 78, no. 5, Article ID 051502, 2008.

[39] T. C. Hales, An overview of the Kepler conjecture. In: arXiv. 2002, https://arxiv.org/abs/math/9811071v2.

[40] C. Song, P. Wang, and H. A. Makse, "A phase diagram for jammed matter," *Nature*, vol. 453, no. 7195, pp. 629–632, 2008.

[41] C. F. Bohren and D. R. Huffman, *Absorption and Scattering of Light by Small Particles*, Wiley, New York, NY, USA, 1998.

[42] V. E. Fertman, *Magnetic Fluids Guidebook: Properties and Applications*, Taylor & Francis, Olympia, Wash, USA, 1990.

[43] J. D. Mayo, 2014, Stabilized reversible polymer composition. U.S. patent application 2014/0353549 A1.